https://doi.org/10.1016/j.apsusc.2020.147694

Highly (*100*)-Orientated SnSe Thin Films Deposited by Pulsed-Laser Deposition

Xiangnan Gong[a], Menglei Feng[b], Hong Wu[b], Hongpeng Zhou[b], Chunhung Suen[c], Hanjun Zou[a], Lijie Guo[b], Kai Zhou[a], Shijian Chen[b], Jiyan Dai[c*], Guoyu Wang[d*], Xiaoyuan Zhou[a, b*]

a. Analytical and Testing Center, Chongqing University, Chongqing 401331, China.

b. College of Physics, Chongqing University, Chongqing 401331, China.

c. Department of Applied Physics, The Hong Kong Polytechnic University, Hong Kong, China.

d. Chongqing Institute of Green and Intelligent Technology, Chinese Academy of Sciences, Chongqing 400714, China.

Keywords: SnSe, Thin films, Pulsed laser deposition, Thermal annealing, Angle-resolved polarized Raman spectra

* Corresponding author.

E-mail: xiaoyuan2013@cqu.edu.cn (Xiaoyuan Zhou)

E-mail: guoyuw@cigit.ac.cn (Guoyu Wang)

E-mail: jiyan.dai@polyu.edu.hk (Jiyan Dai)

Abstract

This work aims at improving the quality of the highly (*100*)-orientated SnSe thin films for thermoelectric applications. The as-deposited films were obtained by controlling the basic parameters including target-to-substrate distance, deposition time and growth temperature through pulsed-laser deposition. The films quality was further improved by vacuum thermal annealing. The microstructure and crystalline structure of the films were studied by X-ray photoelectron spectroscopy, X-ray diffraction, electron probe micro-analyzer, electron back-scatter diffraction, atomic force microscope and Raman spectroscopy. The SnSe thin films grown on SiO_2/Si substrate at 673 K followed by thermal annealing at 673 K for 30 min show the best crystal quality and uniform orientation with mirror-like surface, and the corresponding Seebeck coefficient and power factor are about 383 μV/K and 15.4 μW/m·K^2, respectively. Angle resolved polarized Raman spectroscopy proved that the surface of the SnSe films is the b-c plane with preferred (*100*) orientation crystalline over a large area, providing an important way to prepare thermoelectric thin film devices by pulse laser deposition.

Keywords

SnSe, Thin films, Pulsed laser deposition, Thermal annealing, Angle-resolved polarized Raman spectra

Introduction

Thermoelectric materials (TE) are widely concerned and studied because they can be used in thermoelectric power generation, refrigeration and waste heat recovery based on the Seebeck and Peltier Effects [1-4]. The TE device exhibits many attractive advantages, including small size, light weight, controllable, cleanness without any environmental pollution, long service life [5]. Currently, the most commercially available materials for the thermoelectric industry are bismuth telluride (Bi_2Te_3-based) and lead telluride (PbTe-based) thermoelectric semiconductor materials [3]. However, it remains a significant challenge to realize the widespread application of this kind of devices due to the use of expensive rare, heavy metal toxic materials. Therefore, it is particularly important to seek the thermoelectric semiconductor materials with abundant earth, non-toxic and high performance.

Recently, tin selenide (SnSe), an environmentally friendly TE materials, has been received much attention due to its intrinsically low thermal conductivity and record high performance [6-13]. Zhao et al. have established the world record performance with dimensionless figure of merit ($zT = S^2\sigma T/\kappa$) values of 2.6 and 2.3 at 923 K along the b- and c-axis, respectively [6], owing to the intrinsic low thermal conductivity coupled with a high hole mobility, where S is the Seebeck coefficient, σ is the electrical conductivity, and T is the absolute temperature. However, it is a big challenge to apply SnSe single crystals in practical TE devices due to the poor mechanical properties, complex crystal growth conditions, and high production costs. Therefore, efforts have been focused on growing and preparing high TE performance of polycrystalline SnSe with good mechanical property [14, 15]. Although it is easier to grow polycrystalline materials than single crystal, the main problem of polycrystalline materials is their relatively poor texture and orientation, which seriously affects the carrier mobility and overall performance.

Since L. D. Hicks and M. S. Dresselhaus proposed that the low dimensionality of quantum well superlattice materials can greatly improve the zT value, the study of TE thin films has been promoted for modern micro-thermoelectric devices, such as microchips, minifridges, autonomous wireless sensors and wrist watches [16, 17]. To

date, various of techniques have been used to fabricate SnSe thin films. M. R. Burton et al. reported the first thermoelectric generator based on SnSe films grown via a thermal evaporation method [18]. S. Anwar et al. synthesized SnSe thin films by spray pyrolysis technique in a simple and low-cost way [19]. α-SnSe thin films produced by selenization of magnetron sputtered tin precursors was reported by V. Reddy et al [20]. Among these techniques, the texture of the films is not well controlled, leading to a decrease in carrier mobility, similar in polycrystalline materials. Wang et al. reported the SnSe (111) film with a rock-salt phase which was epitaxially grown on Bi_2Se_3 surface by molecular beam epitaxy (MBE) method [21]. But, its complexity and high cost limited the widespread application. Pulsed laser deposition (PLD) is an effective technique for producing high quality thin film. T. Inoue et al. synthesized SnSe films on three kinds of different single-crystalline substrates by PLD using Se-rich targets [22], B. E. Matthews et al. also used PLD method to fabricate polycrystalline thin films of the metastable heterostructural $Sn_{1-x}Ca_xSe$ on amorphous SiO_2 substrate [23]. Therefore, it is particularly important to prepare large-area highly oriented SnSe films through a relatively simple PLD process.

In the present work, smooth, continuous and large area of highly-orientated SnSe thin films were deposited by the PLD technique. Post-annealing process was performed at various temperatures to further improve the crystalline quality. Thin films were characterized using X-ray photoelectron spectroscopy (XPS), X-ray diffraction (XRD), electron-probe micro-analyzer (EPMA), electron back-scatter diffraction (EBSD), atomic force microscope (AFM) and Raman spectroscopy for a better understanding of the SnSe thin films. Growing (*100*)-oriented crystalline SnSe thin films over a large area by PLD technique provides an important way to prepare thermoelectric thin film devices in the future.

2. Experiment method

2.1 Target and substrates

Pure Sn granules (99.999%) and Se powder (99.99%) were weighed carefully according to the stoichiometry of Sn : Se = 1.0 : 1.1 ($SnSe_{1.1}$) [22, 24], and the samples were loaded into quartz tube and sealed under 5×10^{-4} Pa. The tube was heated up to

1273 K over 12 hours, kept at that temperature for 10 hours, and then the furnace cooled to the room temperature subsequently. The obtained ingots (15 g) were crushed into powder, and it was densified to be the target by spark plasma sintering (SPS) with a graphite die (Φ = 2 inch) at 730 K for 5 minutes under a pressure of 45 MPa. Substrates with dimensions of 12 × 12 mm^2 consisted of p-type Si wafers coated with a 200 nm film of thermal silicon dioxide. The substrates were pre-cleaned with neutral detergent and deionized water and then they were ultrasonically cleared in acetone and anhydrous ethanol for 30 minutes, respectively.

2.2 Thin films deposition and annealing

Thin films of SnSe were grown by a self-designed pulse laser deposition (PLD, CHI-VAC Research & Development Co., Ltd) system. UV pulses (duration 15 ns) from a KrF excimer laser (Coherent, Lambda Physik COMPexPro201F, λ = 248 nm, 5 Hz repetition rate) were focused on the $SnSe_{1.1}$ target. Prior to thin film deposition, pre-sputtering process was done. A baffle was first placed between the target and the substrate, and the surface of the target was ablated with 3000 pulses (5 minutes) under vacuum with the 5 Hz repetition, to remove native oxides and contaminants on the surfaces of the target. Afterward the fresh SnSe exposed. The target rotates in the opposite direction from the substrate and the vacuum of the chamber was kept around 2×10^{-4} Pa. The optimized deposition conditions were used for deposition SnSe on SiO_2/Si substrate has been described in **Table 1**.

The as-deposited SnSe thin films were loaded into the quartz tubes and sealed under 2×10^{-5} Pa. Then tubes were placed in the middle of the furnace (KSL-1200X) to make sure the actual annealing temperature is close to the setup temperature as 373, 473, 573, 623, 673, and 773 K with a 5 K/min of heating ramp. The soaking time is 30 min for all samples, and then cooled to room temperature naturally. The effect of annealing temperature on thin film quality, orientation, distribution and morphology of the as-deposited films was studied. Temperature-dependent thermoelectric properties of these SnSe films were also characterized and analyzed.

2.3 Characterizations and analysis

Structural Characterization: The crystal structure of the resultant thin films was

characterized by X-ray diffraction (XRD) with Cu K_α radiation (λ = 1.5418 Å). Additionally, either a PANalytical X'pert or a Rigaku Smartlab diffractometer was used with similar parallel beam optics. Out-of-plane ω scans ($2\theta = 31.2°$) as well as in-plane pole figure performed with the Rigaku Smartlab instrument.

Micro-Raman spectroscopy was carried out in backscattering geometry using a confocal Raman microscope (Horiba HR Evolution) equipped with continues wave green laser (λ = 532 nm) and 100 × objective. The spectrum was recorded over the range of 40 cm^{-1} to 200 cm^{-1} under 1800 groove/cm holographic grating. The laser power on the sample was adjusted to ≤ 0.2 mW to avoid thermal effect and the acquisition time was 300 s for each spectrum. For angle resolved polarized Raman spectroscopy (ARPRS), a polarizer was placed between incident laser and film, an analyzer was placed between edge filter and detector to obtain the parallel and perpendicular polarization configuration.

Morphological Characterization: The morphology and roughness of SnSe films were measured by AFM (Asylum Research, MFP-3D). EBSD was collected with a NordlysMax^2 detector (Oxford Instruments) integrated with a JEOL JSM-7800F FESEM system. The acceleration voltage was 15 kV and the sample tilted at 70°. The crystallographic orientation data was collected using the Aztec EBSD data acquisition software and post-analyzed using the HKL Channel 5 package for crystallographic orientation mapping.

Photoelectron Spectroscopy: Surface analysis of the films was performed on an X-ray photoelectron spectroscopy (Thermo Scientific EscaLab 250Xi) using a monochromatized Al anode x-ray source ($h\nu$ = 1486.6 eV) equipped with an ion sputter-gun. The ultra-high vacuum chamber with a base pressure of 1×10^{-10} mbar. Sputtering was performed with 1 kV Ar^+ for 30 s leading to a typical sputtering depth of 1 nm. As a result, the SnSe film surface was exposed and the possible contaminations such as C and O were partially removed. The resolution was determined to be 0.43 eV, which gives an uncertainty of ± 0.05 eV for the banding energy. The spectra were calibrated by the C 1s peak at 284.6 eV. XPS core levels of Sn and Se were not affected by the measurement angle, and the data shown were measured at 90° (perpendicular to the

substrate).

Electron probe micro-analyzer (EPMA, JXA-8530F Plus, JEOL, Japan) was used to determine the distributions of Sn and Se in the annealing SnSe thin film with a spatial resolution of 1 mm. The EPMA was equipped with fives X-ray spectrometers and operated under an acceleration voltage of 8 kV and 10 nA stabilized beam. Full wavelength dispersive spectrometry (WDS) mode was employed.

The thicknesses of the SnSe films on SiO_2/Si substrates were determined by cross-sectional scanning electron microscopy (SEM) (Thermo Fisher, Quattro S), and the uniformity of film thickness was characterized by a film thickness gauge (F50, Filmetrics, USA) with a 1.5 mm spot size.

The Seebeck coefficient and the conductivity of the films were characterized by the MRS system from JouleYacht at a temperature range from RT to 573 K; the Seebeck coefficient was measured by a dynamic method, and the conductivity was measured by a four-point probe method.

3. Result and discussion

Both Sn and Se doublets from the as-deposited SnSe thin film were examined by the high resolution XPS and the results are shown in **Figure 1**(a) and (b), respectively. Distinctive Sn 3d and Se 3d peaks indicate the orthorhombic phase in our SnSe thin film, where the $3d_{3/2}$ and $3d_{5/2}$ peaks for Sn appear at 493.55 eV and 485.14 eV, respectively, with a separation of 8.41 eV. While $3d_{3/2}$ and $3d_{5/2}$ peaks for Se appear at 53.89 eV and 53.02 eV, respectively, with a separation of 0.87 eV, indicating that the Sn-Se bonding is agree with the binding energies of Sn^{2+} and Se^{2-} in the previous reports [18]. It is apparent that the sharp peaks with full width half maximum (FWHM) < 1 eV indicate a single bonding environment with no evidence of a Sn^{4+} peak at 486.7 eV or a Se^{4+} peak in the region of 58~59 eV [25].

The distributions of Sn and Se in the 673 K annealed film were unambiguously revealed by EPMA color mapping as shown in **Figure 1**(c, d). One can see that the two elements are evenly distributed over the 10×10 mm^2 area, and a random line is selected for scanning to get composition ratios of the sample. **Figure 1**(e) shows that the Sn : Se atom ratio is around 1, suggesting a stoichiometric proportion.

XRD patterns for the SiO_2/Si substrate and as-deposited thin film were shown in **Figure 1**(f). According to XRD analysis, the peaks in these patterns with negligibly weak in accord with the JCPDS 48-1224, which is the low temperature orthorhombic phase (space group *Pnma* (#62)) of SnSe. As depicted, the main peaks are corresponding to the (*h00*) preferential atomic planes of SnSe [26]. This texturing was further demonstrated macroscopically by the strong intensity at the center of the (400) pole figure for the SnSe thin film as shown in **Figure 2**(a), which represents normal hemispherical stereographic projections of the specific crystal planes, and only (400)-orientation grains can be observed clearly [26]. Furthermore, the orientation factor *f* of (*h00*) plane using Lotgering's method had been calculated from the XRD data to estimate the degree of orientation for the annealed SnSe thin films [26, 27]. It was evaluated by following equations:

$$f = \frac{p - p_0}{1 - p_0} \tag{1}$$

$$p = \frac{\sum I(h00)}{\sum I(hkl)} \tag{2}$$

$$p_0 = \frac{\sum I_0(h00)}{\sum I_0(hkl)} \tag{3}$$

where I and I_0 are the intensities of the XRD peaks for the sample and the reference, p and p_0 represent the relative quantity of *(h00*) reflections to that of all reflections for the sample and the reference, respectively. The estimated orientation factor f of the current SnSe thin film achieves an excellent orientation factor over 0.99 due to the super strong (*h00*) intensity, indicating an excellent textured structure close to the ideal crystals. Owing to the highly textured structure, the SnSe films would exhibit high Hall mobility to get good electrical properties [28].

Electron backscatter diffraction (EBSD) images were obtained to further investigate the SnSe grain orientation deposited by PLD technique. Compared to the macroscopic measurement and analysis in XRD, EBSD is more sensitive to the surface texture in microscopic measurement [29]. **Figure 2**(b) shows an EBSD image quality (IQ) map from the center region of the SnSe film annealed at 623 K which is generally representative of the microstructure observed in the films, the microstructure of the grain boundary is clearly observed from the high resolution of a magnified region.

Figure 2(c) shows the 256 colour relative Euler map of the corresponding area, in which the primary colors are proportional to the three Euler angles provided by the software. In many cases, regions of similar orientation have similar colors [30]. **Figure 2**(d) shows the corresponding EBSD inverse pole figure (IPF) orientation map, color represents the crystallographic orientation of the annealed film along with the (100) direction [31, 32]. Black region stands for non-indexed point areas caused by small size of grains that are below the effective spatial resolution.

The morphology of the SnSe thin films varied from different annealing temperatures were also studied by AFM as shown in **Figure 3**(a-g). The size of grains grows from few nanometers to more than 300 nm, and the shape of grains changes from pellet to prismatic during increasing annealing temperature from room temperature to 773 K, together with an increase of the overall roughness. R_{RMS} (roughness root mean squared) were measured on the 1 × 1 μm^2 AFM profile for each sample and yielded values from 0.6 nm to 5.8 nm in **Figure 3**(h). The progression of R_{RMS} roughness for as-deposited and annealed SnSe films is concomitant with crystallite size changes indicating grain growth directly influences the surface roughness. Higher surface roughness can be expected for larger grain cluster due to larger height difference between peak and base of grains.

Figure 4(a-f) show the thickness of the annealed SnSe films around 400 nm at different annealing temperatures by cross-sectional SEM back-scattering images at high magnification. The low magnification cross-sectional images are shown in **Figure S1**. **Figure 4**(g) shows the thickness uniformity of the PLD SnSe thin film on the 10 × 10 mm^2 SiO_2/Si substrate which annealed at 673 K, evaluated by mapping its thickness with 21 points by film thickness gauge at room temperature. The film thickness on the entire substrate is around 407 ± 20nm, and the non-uniformity can be further improved by centering the substrate when deposition process.

The crystallinity of the as-deposited and annealed films was studied by XRD. **Figure 5**(a) shows the θ-2θ XRD patterns of the SiO_2/Si substrate, the as-deposited and annealed films in vacuum with various annealing temperature, respectively. The as-deposited films were improved from target-substrate distance, deposition time and

grown temperature, respectively as shown in **Figure S2**. **Figure 5**(b) shows an expand view of the (400) plane in the range of 30.4 ~ 32.0° to observe the (400) peak intensities, positions, and its FWHMs (the full width at half maximum) clearly. On the one hand, the intensity of the (400) peaks increases by the annealing temperature from RT to 673 K, and then decreases at higher annealing temperature. The sharp and strong peaks of the annealed films were attributed to the improved crystallinity caused by the annealing process, but became worse at higher annealing temperature. On the other hand, the FWHMs of the (400) peaks decrease by the annealing temperature from RT to 673 K, and then increase at higher annealing temperature depicted in the inset of **Figure 5**(b), indicating an improvement in the crystal quality of the SnSe thin films by the annealing process and then became worse at higher temperature. As shown in the **Figure 5**(b), the main peak of (400) shifts to the higher angle when the annealing temperature increased. Based on the Bragg' law, $2d\sin\theta = n\lambda$, we can conclude that the interplanar spacing d decreases when annealing temperature increase, indicating the residual stress is released when the annealing temperature increases. As such, the experimental results are in good agreement with the theoretical expectations as obviously shown in the inset of **Figure 5**(b) in the temperature range from 473 K to 573 K. The lattice parameters of SnSe films annealed at different temperature were refined from the XRD data as shown in **Table 2**. We noticed that the lattice parameters of SnSe continuously evolved with the increasing temperature, all samples were *Pnma* phase [33]. **Figure 5**(c) shows the XRD rocking curves of the annealing temperature effect on the SnSe thin films, the narrowest FWHM of (400) peak is 1.18° at 673 K, strongly supporting that 673 K is the best annealing temperature to improve the SnSe thin film in our experiment. As a result, annealing treatment can effectively improve the crystallization quality of the film.

To confirm the phase purity and the crystalline quality of the SnSe thin films, Raman spectroscopy analysis was carried out due to this method is more sensitive and non-destructive to compositional and structural changes in the materials [34]. **Figure 5**(d) shows the Raman spectra of the as-deposited and different annealed temperatures of SnSe thin film in a range of 40-200 cm^{-1}. The Raman peaks can be detected at 70, 104, 127 and 151 cm^{-1}, respectively, which are consistent with previously reported

values, and these four peaks are assigned as A_g^1, B_{3g}, A_g^2 and A_g^3, respectively [35-38]. The inset depicted that the A_g^1 mode peak position and its FWHM varied as different annealing temperatures. The A_g^1 peak position jumped up 2.33 cm^{-1}, while the A_g^1 peak FWHM drops 4.41 cm^{-1} when temperature increases from 473 K to 573 K. This result is in accordance with the XRD analysis to illustrate that the crystalline quality of the film is improved by the annealing process [39, 40]. The uniformity of the SnSe structure had been characterized by Raman mapping shown in the **Figure S3**(a), totally 20 Raman spectra were obtained from each point depicted in **Figure S3**(b) for the 673 K annealed film.

To demonstrate and confirm the correlation with the thin film orientation, ARPRS was carried out on the best thin film which is annealed at 673 K shown in **Figure 6**. It was measured by adjusting the relative angles between the polarization direction of excitation laser and thin film orientation to probe the anisotropic Raman response in both $\overline{z}(xy)z$ (perpendicular) and $\overline{z}(xx)z$ (parallel) configurations. The Raman scatter intensity *I*, which is proportional to $I = |e_i \cdot R \cdot {e_s}^T|$, the unitary vectors e_i and e_s refer to the incident and scattered laser polarizations, respectively. *R* is the Raman tensor of Raman active modes. In our backscattering geometry configuration, e_i can be expressed as $(0, \cos\theta, \sin\theta)$, e_s can be expressed as $(0, \sin\theta, \cos\theta)$ and $(0, -\sin\theta, \cos\theta)$ under the parallel polarization configuration and perpendicular-polarization configuration, respectively. From group theory, the two Raman tensors can be written as follows [36, 37, 41]:

$$R(A_g) = \begin{pmatrix} a & 0 & 0 \\ 0 & b & 0 \\ 0 & 0 & c \end{pmatrix} \quad R(B_g) = \begin{pmatrix} 0 & 0 & 0 \\ 0 & 0 & g \\ 0 & g & 0 \end{pmatrix}$$

Where a, b, c, and g are the Raman tensor elements. When the incident laser beam is polarized by θ with respect to the zigzag direction, the corresponding Raman intensity I varies with θ are further expressed as follows:

$$I(A_g, \|) = (a\cos^2\theta + c\sin^2\theta)^2 \qquad (4)$$

$$I(A_g,\perp)=\frac{(c-b)^2}{4}\sin^2 2\theta \quad (5)$$

$$I(B_g,\|)=g^2\sin^2 2\theta \quad (6)$$

$$I(B_g,\perp)=g^2\cos^2 2\theta \quad (7)$$

The sample was perpendicular to the laser beam fixed on the stage, and the relative angle θ is the rotation angle of the incident laser polarization. Under parallel polarization configuration from **Eq.** (4), the period of A_g mode is 180° and the maximum Raman intensity $I(A_g)$ is c^2 when $\theta = 90°$, a^2 when $\theta = 0°$, respectively. From **Eq.** (6), the period of B_g mode is 90° and the maximum Raman intensity $I(B_g)$ is g^2 when $\theta = 45°$. Under perpendicular polarization configuration from **Eq.** (5), the period of A_g mode is 90° and the maximum Raman intensity $I(A_g)$ is $\frac{(c-b)^2}{4}$ when $\theta = 45°$. From **Eq.** (7), the period of B_g mode is 90° and the maximum Raman intensity $I(B_g)$ is g^2 when $\theta = 0°$. It can be concluded that the position of extrema and polarized periodicity are matched well after comparing the above theoretical calculation and experiment data. As a result, the A_g mode under parallel polarization configuration is special to identify the zigzag direction or armchair direction of SnSe thin film from Raman polarization intensity diagrams and **Eq.** (4). From the above, the Raman intensities of A_g^1, B_{3g}, A_g^2 and A_g^3 modes in SnSe show obvious periodic variation (90° or 180°) with the incident laser polarization angle under both parallel and cross-polarization configurations, these vibration modes show different features of variation. All the results of the ARPRS match well with symmetry selection rules based on the Raman tensors, demonstrating the strong anisotropic nature of the annealed SnSe thin films.

As depicted in **Figure 7**(a), the Seebeck coefficients of the samples annealed at lower temperature (RT, 373 K and 473 K) varied from positive to negative, indicating that the films changed from p-type to n-type semiconductors with increasing

temperature in the range of 300-573 K. This special behavior may be caused by the mixing of amorphous and nanocrystalline, the seebeck coefficient showed the stable p-type behavior when the annealing temperature increase up to 573 K, despite the seebeck coefficient value decrease a little bit for the 673 K sample. **Figure 7**(b) showed that the electrical conductivity of all the films increased with the annealing temperature in the range of 300-575 K, and the 673 K sample showed almost the highest value 183 S/m at 573 K. This trend and the maximum value are almost the same as SnSe films in the literature at this temperature range [18]. **Figure 7**(c) showed the power factor (PF = $S^2 \cdot \sigma$) values as a function of temperatures. For our best SnSe thin film (673 K sample), the PF value is about 0.26 $\mu Wm^{-1}K^{-2}$ at 304 K, 15.38 $\mu Wm^{-1}K^{-2}$ at 573 K, respectively. The main reason to hinder the further improvement of thermoelectrical performance is the high electrical resistivity of our films. The electrical resistivity is even higher than 3×10^5 $\mu\Omega \cdot m$ at 392 K which is almost beyond the limit of the thermoelectrical measurement system. The above results suggest that the optimal annealing temperature for the PLD SnSe thin film is 673 K, which allows for good crystallinity and appropriate film texture simultaneously to achieve the aim of high thermoelectric performance.

4. Conclusion

In this work, multiple advanced characterizations have been used to confirm that we have achieved deposition of centimeter-scale, mirror-like (*100*)-preferred orientation SnSe films by PLD technique with post-annealing. Remarkably, the annealing at 673 K resulted in highly crystalline and smooth SnSe films. The present method opens new avenues for the use of SnSe through scalable, high-quality films with readily controlled thickness and should be easily adaptable for both fundamental and applied studies in thermoelectric.

5. Acknowledgments

This work was financially supported in part by the National Natural Science Foundation of China (Grant Nos. 51772035, 11604032, 51472036), the Fundamental Research Funds for the Central Universities (106112017CDJQJ308821). The work

conducted at the Chongqing Institute of Green and Intelligent Technology, Chinese Academy of Sciences is also supported by Key Research Program of Frontier Sciences, CAS, Grant No. QYZDB-SSWSLH016. This work is sponsored by Natural Science Foundation of Chongqing, China, cstc2019jcyj-msxmX0554, and the Starting Research Fund from the Chongqing University. Xiangnan Gong would like to thank Professor Yulong Liu (Institute of Physics, Chinese Academy of Science) for useful discussion of the results. Dr. Yang Zhou (Analytical and Testing Center) in Chongqing University for her helpful measurement in EPMA.

References

[1] L.E. Bell, Cooling, heating, generating power, and recovering waste heat with thermoelectric systems, Science, 321 (2008) 1457-1461.

[2] J.R. Sootsman, D.Y. Chung, M.G. Kanatzidis, New and old concepts in thermoelectric materials, Angew. Chem. Int. Ed., 48 (2009) 8616-8639.

[3] D.M. Rowe, CRC handbook of thermoelectrics, CRC press, 2018.

[4] G.J. Snyder, E.S. Toberer, Complex thermoelectric materials, Nat. Mater., 7 (2008) 105-114.

[5] Z. Lin, C. Hollar, J.S. Kang, A. Yin, Y. Wang, H.Y. Shiu, Y. Huang, Y. Hu, Y. Zhang, X. Duan, A Solution Processable High-Performance Thermoelectric Copper Selenide Thin Film, Adv. Mater., 29 (2017).

[6] L.-D. Zhao, S.-H. Lo, Y. Zhang, H. Sun, G. Tan, C. Uher, C. Wolverton, V.P. Dravid, M.G. Kanatzidis, Ultralow thermal conductivity and high thermoelectric figure of merit in SnSe crystals, Nature, 508 (2014) 373-377.

[7] X. Wang, X. Zhao, C. Hu, Y. Zhang, B. Song, L. Zhang, W. Liu, Z. Lv, Y. Zhang, J. Tang, Y. Sui, B. Song, Large lateral photovoltaic effect with ultrafast relaxation time in SnSe/Si junction, Appl. Phys. Lett., 109 (2016).

[8] C. Zhang, H. Yin, M. Han, Z. Dai, H. Pang, Y. Zheng, Y.Q. Lan, J. Bao, J. Zhu, Two-dimensional tin selenide nanostructures for flexible all-solid-state supercapacitors, ACS Nano, 8 (2014) 3761-3770.

[9] K. Peng, X. Lu, H. Zhan, S. Hui, X. Tang, G. Wang, J. Dai, C. Uher, G. Wang, X. Zhou, Broad temperature plateau for high ZTs in heavily doped p-type SnSe single crystals, Energy Environ. Sci., 9 (2016) 454-460.

[10] N.A. Rongione, M. Li, H. Wu, H.D. Nguyen, J.S. Kang, B. Ouyang, H. Xia, Y. Hu, High-Performance Solution-Processable Flexible SnSe Nanosheet Films for Lower Grade Waste Heat Recovery, Adv. Electro. Mater., (2019).

[11] S. Yuan, Y.H. Zhu, W. Li, S. Wang, D. Xu, L. Li, Y. Zhang, X.B. Zhang, Surfactant-Free Aqueous Synthesis of Pure Single-Crystalline SnSe Nanosheet Clusters as Anode for High Energy- and Power-Density Sodium-Ion Batteries, Adv. Mater., 29 (2017).

[12] K. Peng, B. Zhang, H. Wu, X. Cao, A. Li, D. Yang, X. Lu, G. Wang, X. Han, C.

Uher, X. Zhou, Ultra-high average figure of merit in synergistic band engineered Sn x Na 1− x Se 0.9 S 0.1 single crystals, Mater. Today, 21 (2018) 501-507.

[13] L. Huang, J. Lu, D. Ma, C. Ma, B. Zhang, H. Wang, G. Wang, D.H. Gregory, X. Zhou, G. Han, Facile in situ solution synthesis of SnSe/rGO nanocomposites with enhanced thermoelectric performance, J. Mater. Chem. A, 8 (2020) 1394-1402.

[14] G. Yang, L. Sang, M. Li, S.M. Kazi Nazrul Islam, Z. Yue, L. Liu, J. Li, D.R.G. Mitchell, N. Ye, X. Wang, Enhancing the Thermoelectric Performance of Polycrystalline SnSe by Decoupling Electrical and Thermal Transport through Carbon Fiber Incorporation, ACS Appl. Mater. Interfaces, 12 (2020) 12910-12918.

[15] C. Li, H. Wu, B. Zhang, H. Zhu, Y. Fan, X. Lu, X. Sun, X. Zhang, G. Wang, X. Zhou, High Thermoelectric Performance of Co-Doped P-Type Polycrystalline SnSe via Optimizing Electrical Transport Properties, ACS Appl. Mater. Interfaces, 12 (2020) 8446-8455.

[16] L.D. Hicks, M.S. Dresselhaus, Effect of quantum-well structures on the thermoelectric figure of merit, Phys Rev B Condens Matter, 47 (1993) 12727-12731.

[17] L. Song, J. Zhang, B.B. Iversen, Enhanced thermoelectric properties of SnSe thin films grown by single-target magnetron sputtering, J. Mater. Chem. A, 7 (2019) 17981-17986.

[18] M.R. Burton, T. Liu, J. McGettrick, S. Mehraban, J. Baker, A. Pockett, T. Watson, O. Fenwick, M.J. Carnie, Thin Film Tin Selenide (SnSe) Thermoelectric Generators Exhibiting Ultralow Thermal Conductivity, Adv. Mater., 30 (2018) e1801357.

[19] S. Anwar, S. Gowthamaraju, B.K. Mishra, S.K. Singh, A. Shahid, Spray pyrolysis deposited tin selenide thin films for thermoelectric applications, Mater. Chem. Phys., 153 (2015) 236-242.

[20] V.R. Minnam Reddy, G. Lindwall, B. Pejjai, S. Gedi, T.R.R. Kotte, M. Sugiyama, Z.-K. Liu, C. Park, α-SnSe thin film solar cells produced by selenization of magnetron sputtered tin precursors, Sol. Energy Mater. Sol. Cells, 176 (2018) 251-258.

[21] Z. Wang, J. Wang, Y. Zang, Q. Zhang, J.A. Shi, T. Jiang, Y. Gong, C.L. Song, S.H. Ji, L.L. Wang, L. Gu, K. He, W. Duan, X. Ma, X. Chen, Q.K. Xue, Molecular Beam Epitaxy-Grown SnSe in the Rock-Salt Structure: An Artificial Topological Crystalline

Insulator Material, Adv. Mater., 27 (2015) 4150-4154.

[22] T. Inoue, H. Hiramatsu, H. Hosono, T. Kamiya, Heteroepitaxial growth of SnSe films by pulsed laser deposition using Se-rich targets, J. Appl. Phys., 118 (2015).

[23] B.E. Matthews, A.M. Holder, L.T. Schelhas, S. Siol, J.W. May, M.R. Forkner, D. Vigil-Fowler, M.F. Toney, J.D. Perkins, B.P. Gorman, A. Zakutayev, S. Lany, J. Tate, Using heterostructural alloying to tune the structure and properties of the thermoelectric Sn1−xCaxSe, J. Mater. Chem. A, 5 (2017) 16873-16882.

[24] S. Saini, P. Mele, A. Tiwari, Influence of the planar orientation of the substrate on thermoelectric response of SnSe thin films, J. Phys. Chem. Solids, 129 (2019) 347-353.

[25] A. Naveau, F. Monteil-Rivera, E. Guillon, J. Dumonceau, Interactions of aqueous selenium (-II) and (IV) with metallic sulfide surfaces, Environ. Sci. Technol., 41 (2007) 5376-5382.

[26] S.H. Heo, S. Jo, H.S. Kim, G. Choi, J.Y. Song, J.Y. Kang, N.J. Park, H.W. Ban, F. Kim, H. Jeong, J. Jung, J. Jang, W.B. Lee, H. Shin, J.S. Son, Composition change-driven texturing and doping in solution-processed SnSe thermoelectric thin films, Nat. Commun., 10 (2019) 864.

[27] F.K. Lotgering, Topotactical Reactions with Ferrimagnetic Oxides Having Hexagonal Crystal Structures–I, J. Inorg. Nucl. Chem., 9 (1959) 113-+.

[28] Y. Fu, J. Xu, G.-Q. Liu, J. Yang, X. Tan, Z. Liu, H. Qin, H. Shao, H. Jiang, B. Liang, J. Jiang, Enhanced thermoelectric performance in p-type polycrystalline SnSe benefiting from texture modulation, J. Mater. Chem. C, 4 (2016) 1201-1207.

[29] S.I. Wright, M.M. Nowell, EBSD image quality mapping, Microsc. Microanal., 12 (2006) 72-84.

[30] A.A. Gazder, W. Cao, C.H.J. Davies, E.V. Pereloma, An EBSD investigation of interstitial-free steel subjected to equal channel angular extrusion, Mater. Sci. Eng. A, 497 (2008) 341-352.

[31] S. Suzuki, Features of Transmission EBSD and its Application, Jom, 65 (2013) 1254-1263.

[32] Q. Yin, L. Chen, Enhanced optical properties of Sn-doped Ge2Sb2Te5 thin film with structural evolution, J. Alloys Compd., 770 (2019) 692-700.

[33] C.W. Li, J. Hong, A.F. May, D. Bansal, S. Chi, T. Hong, G. Ehlers, O. Delaire, Orbitally driven giant phonon anharmonicity in SnSe, Nat. Phys., 11 (2015) 1063-1069.
[34] X. Zhang, Q.H. Tan, J.B. Wu, W. Shi, P.H. Tan, Review on the Raman spectroscopy of different types of layered materials, Nanoscale, 8 (2016) 6435-6450.
[35] H.R. Chandrasekhar, R.G. Humphreys, U. Zwick, M. Cardona, Infrared and Raman spectra of the IV-VI compounds SnS and SnSe, Phys. Rev. B, 15 (1977) 2177-2183.
[36] X. Xu, Q. Song, H. Wang, P. Li, K. Zhang, Y. Wang, K. Yuan, Z. Yang, Y. Ye, L. Dai, In-Plane Anisotropies of Polarized Raman Response and Electrical Conductivity in Layered Tin Selenide, ACS Appl. Mater. Interfaces, 9 (2017) 12601-12607.
[37] X.Z. Li, J. Xia, L. Wang, Y.Y. Gu, H.Q. Cheng, X.M. Meng, Layered SnSe nano-plates with excellent in-plane anisotropic properties of Raman spectrum and photo-response, Nanoscale, 9 (2017) 14558-14564.
[38] X. Gong, H. Wu, D. Yang, B. Zhang, K. Peng, H. Zou, L. Guo, X. Lu, Y. Chai, G. Wang, X. Zhou, Temperature dependence of Raman scattering in single crystal SnSe, Vib. Spectrosc., 107 (2020).
[39] X. Hu, J. Tao, S. Chen, J. Xue, G. Weng, Kaijiang, Z. Hu, J. Jiang, S. Chen, Z. Zhu, J. Chu, Improving the efficiency of Sb2Se3 thin-film solar cells by post annealing treatment in vacuum condition, Sol. Energy Mater. Sol. Cells, 187 (2018) 170-175.
[40] A. Kanai, H. Araki, A. Takeuchi, H. Katagiri, Annealing temperature dependence of photovoltaic properties of solar cells containing Cu2SnS3thin films produced by co-evaporation, Phys. Status Solidi B, 252 (2015) 1239-1243.
[41] R. Loudon, The Raman effect in crystals, Adv. Phys., 50 (2001) 813-864.

Table 1 Deposition conditions used for SnSe thin films on SiO_2/Si substrate.

Deposition conditions	**Parameters**
Base Vacuum	2×10^{-4} Pa
Energy fluence	2.0 J/cm^2
Laser wavelength	248 nm
Repetition rate	5 Hz
Pulse duration	15 ns
Target-to substrate distance	45, 55 and 65 mm
Deposition time	2, 5 and 10 min
Substrate temperature	RT, 373, 473, 573, 623, 673 and 773 K
Annealing temperature	373, 473, 573, 623 and 673 K

Table 2 The lattice parameters of SnSe films annealed at different temperature.

Temperature (K)	a (Å)	b (Å)	c (Å)
RT	11.9328	4.4129	4.2928
373	11.9305	4.3972	4.2953
473	11.9329	4.4045	4.2954
573	11.9142	4.3769	4.3042
623	11.8965	4.3788	4.3046
673	11.8953	4.3809	4.3048
773	11.9138	4.4007	4.3048

Figure Captions

Figure 1 (a) Sn 3d XPS peaks, showing the presence of Sn $3d_{3/2}$ (493.55 eV) and Sn $3d_{5/2}$ (485.14 eV); (b) Se 3d XPS peaks, showing the presence of Se $3d_{3/2}$ (53.89 eV) and Se $3d_{5/2}$ (53.02 eV); (c, d) EPMA Sn and Se element distribution maps of the whole sample (10 mm × 10 mm); (e) Atom concentration of Sn and Se corresponding to the line scanning in (c, d). (f) XRD pattern of the SiO_2/Si substrate and the as-deposited SnSe thin film, PDF card is 48-1224.

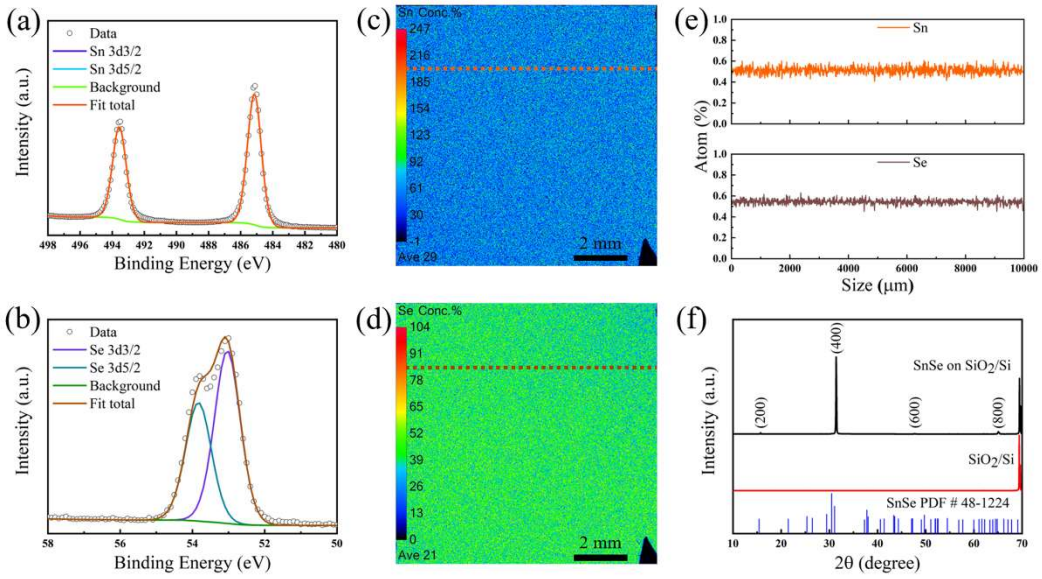

Figure 2 (a) Pole figure; (b) EBSD image quality (IQ) map from the center region of the as-grown SnSe film deposited at 623 K for 10 min, which is generally representative of the microstructure observed in all the as-grown films; (c) Corresponding Euler angle map; (d) Corresponding IPF Z direction map. The scalebar for (b-d) is 1 μm.

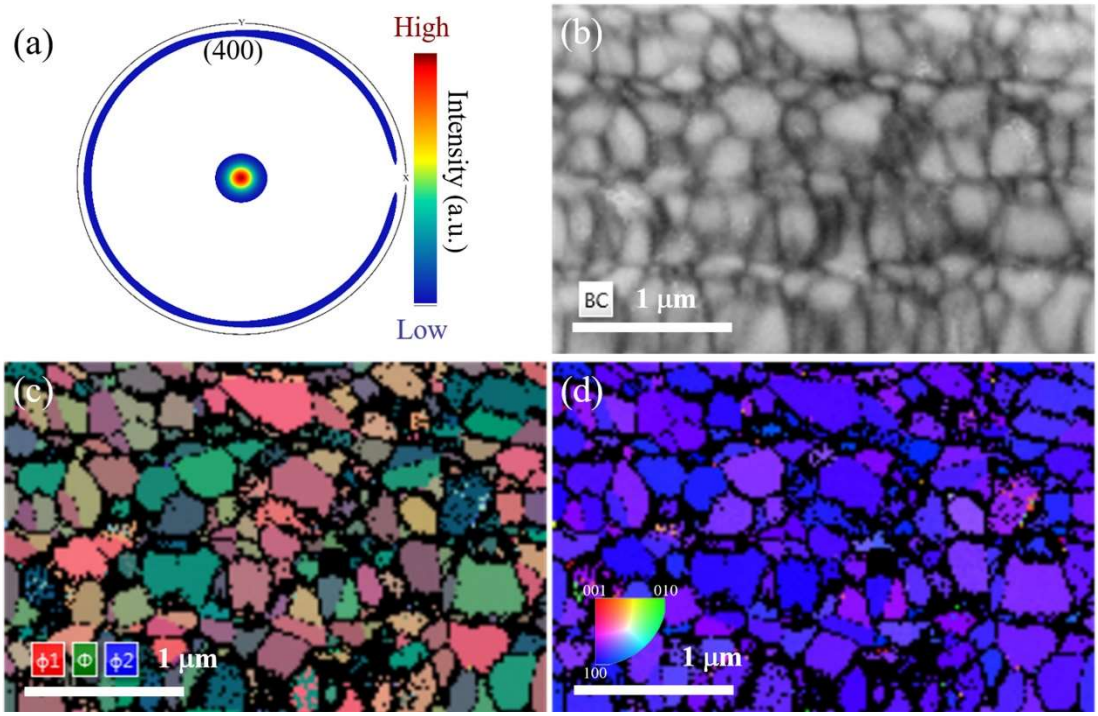

Figure 3 AFM images of as-deposited and annealed thin films. (a) As-deposited, (b) 373 K, (c) 473 K, (d) 573 K, (e) 623 K, (f) 673 K, (g) 773 K, and (h) Histogram of each sample surface roughness. The scalebar for (a-g) is 200 nm.

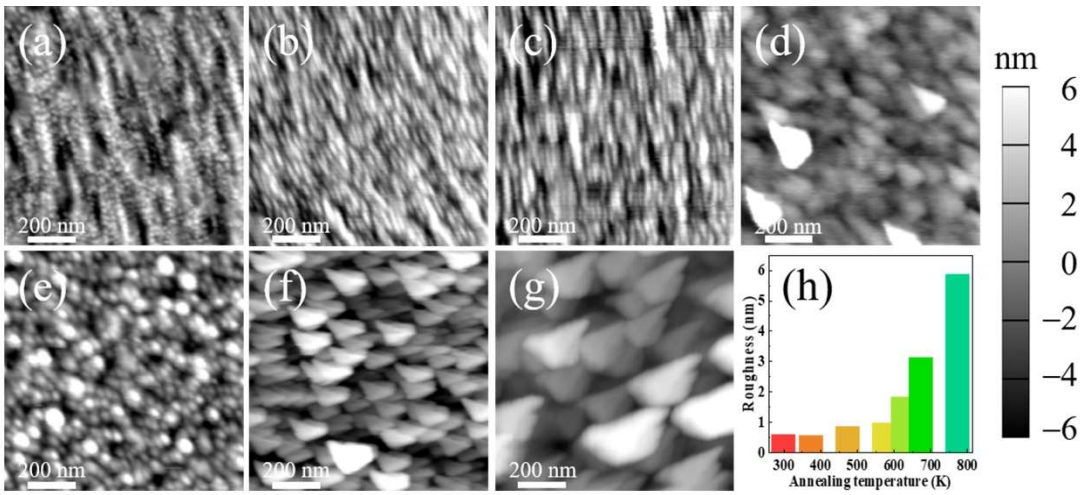

Figure 4 Cross-sectional SEM images of (*l00*)-orientation SnSe thin film. (a) As-deposited, (b) 373 K, (c) 473 K, (d) 573 K, (e) 623 K, (f) 673 K. (g) thickness uniformity of the PLD SnSe thin film annealed at 673 K for 30 min on a 10 × 10 mm^2 SiO_2/Si substrate, as determined by room temperature film thickness gauge mapping.

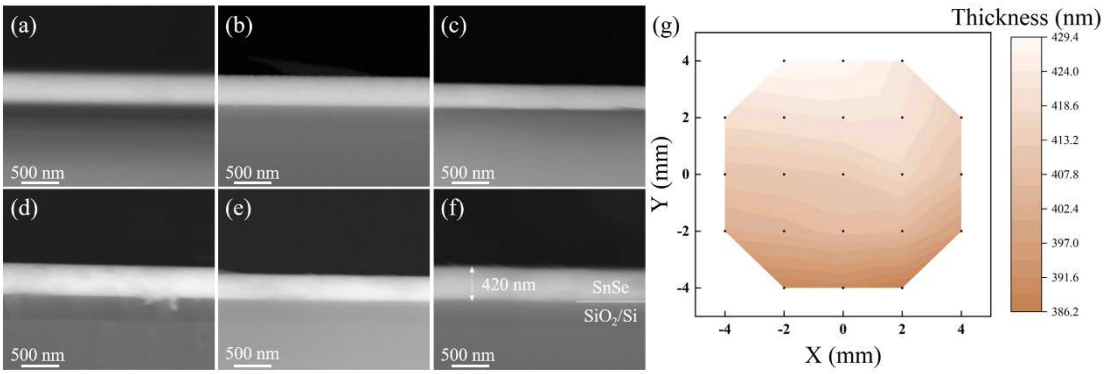

Figure 5 (a) Wide-angle XRD patterns of the substrate, the as-deposited and annealed SnSe films at different temperatures for 30 min; (b) Expand view of the (400) lattice face. The inset shows the zoom of the (400) peak intensities and positions of the different annealing temperature; (c) Rocking curves of each film by the main (400) peak; (d) Raman patterns of the as-deposited and annealed SnSe films at different temperatures for 30 min. The inset shows the relationship between the A_g^1 peak position and annealing temperature, the A_g^1 peak FWHM and annealing temperature.

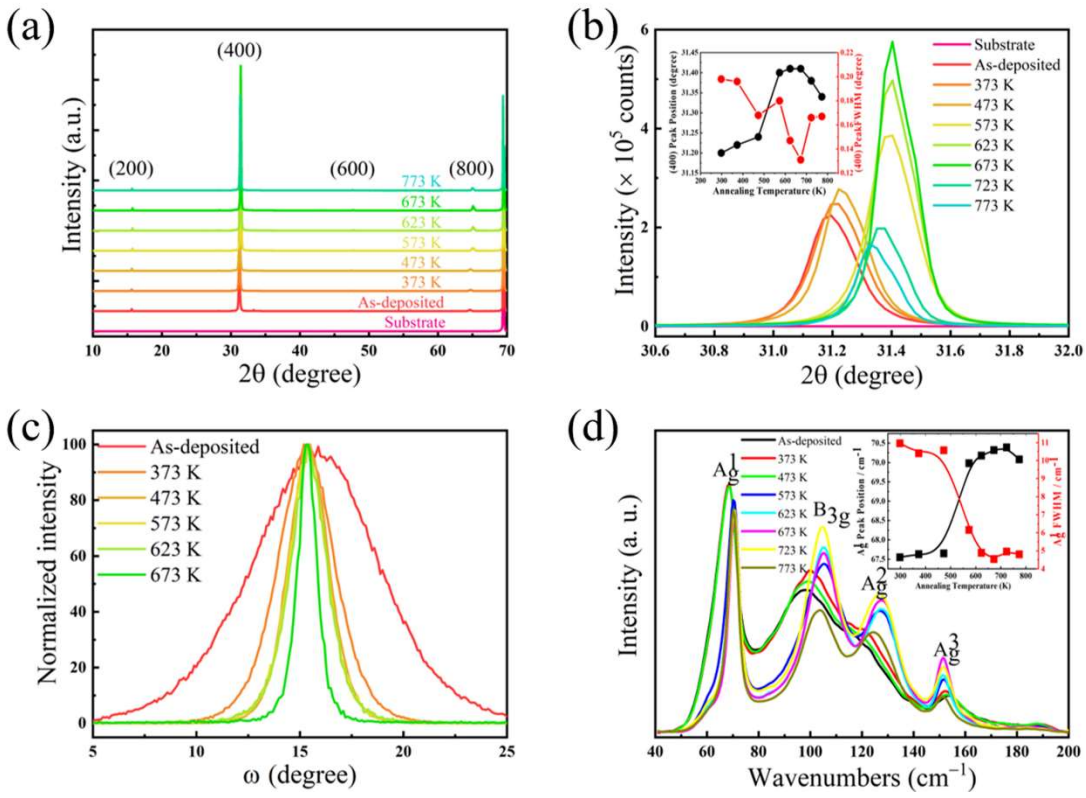

Figure 6 Angle resolved polarized Raman spectroscopy of SnSe thin films. (a-d) depict perpendicular configuration and (e-h) depict parallel configuration, respectively.

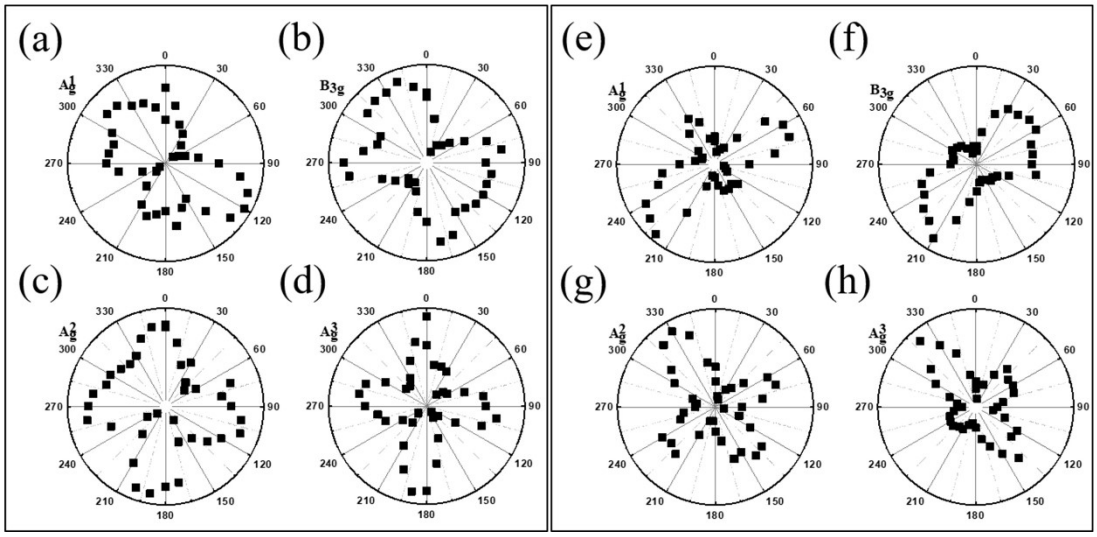

Figure 7 Temperature-dependent thermoelectric properties, (a) Seebeck coefficient (b) electrical conductivity (c) Power factor for the annealed SnSe thin films.

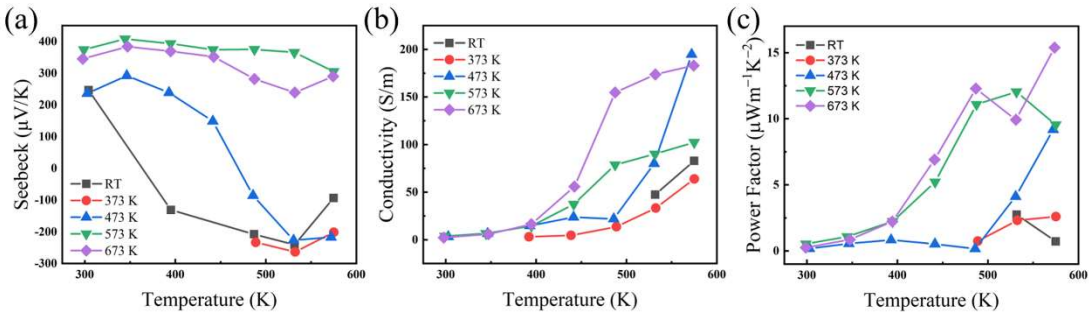

Support Information

Highly (*100*)-Orientated SnSe Thin Films Deposited by Pulsed-Laser Deposition

Xiangnan Gong[a], Menglei Feng[b], Hong Wu[b], Hongpeng Zhou[b], Chunhung Suen[c], Hanjun Zou[a], Lijie Guo[b], Kai Zhou[a], Shijian Chen[b], Jiyan Dai[c*], Guoyu Wang[d*], Xiaoyuan Zhou[a, b*]

a. Analytical and Testing Center, Chongqing University, Chongqing 401331, China.

b. College of Physics, Chongqing University, Chongqing 401331, China.

c. Department of Applied Physics, The Hong Kong Polytechnic University, Hong Kong, China.

d. Chongqing Institute of Green and Intelligent Technology, Chinese Academy of Sciences, Chongqing 400714, China.

* Corresponding author.

E-mail: xiaoyuan2013@cqu.edu.cn (Xiaoyuan Zhou)

E-mail: guoyuw@cigit.ac.cn (Guoyu Wang)

E-mail: jiyan.dai@polyu.edu.hk (Jiyan Dai)

Figure S1 Low magnification of the cross-sectional SEM images of the annealed films at different temperatures (a) As-deposited, (b) 373 K, (c) 473 K, (d) 573 K, (e) 623 K, (f) 673 K.

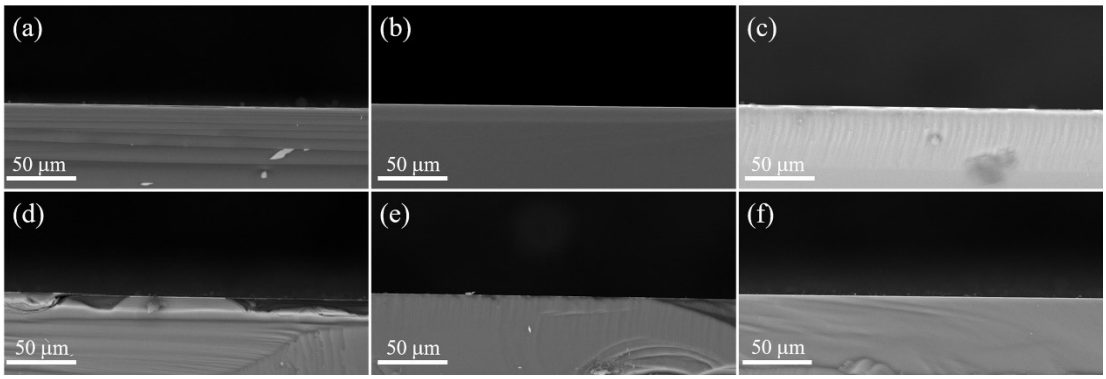

Figure S2 XRD patterns of the as-deposited SnSe thin film crystalline quality improvement from adjusting PLD parameters. (a) target-to-substrate distances, (c) deposition time, (e) grown temperature. The corresponding insets are the (400) lattice face position and FWHM accompany with the improvement parameters. Expanding view of the (400) lattice face intensity are shown in (b), (d) and (e), respectively.

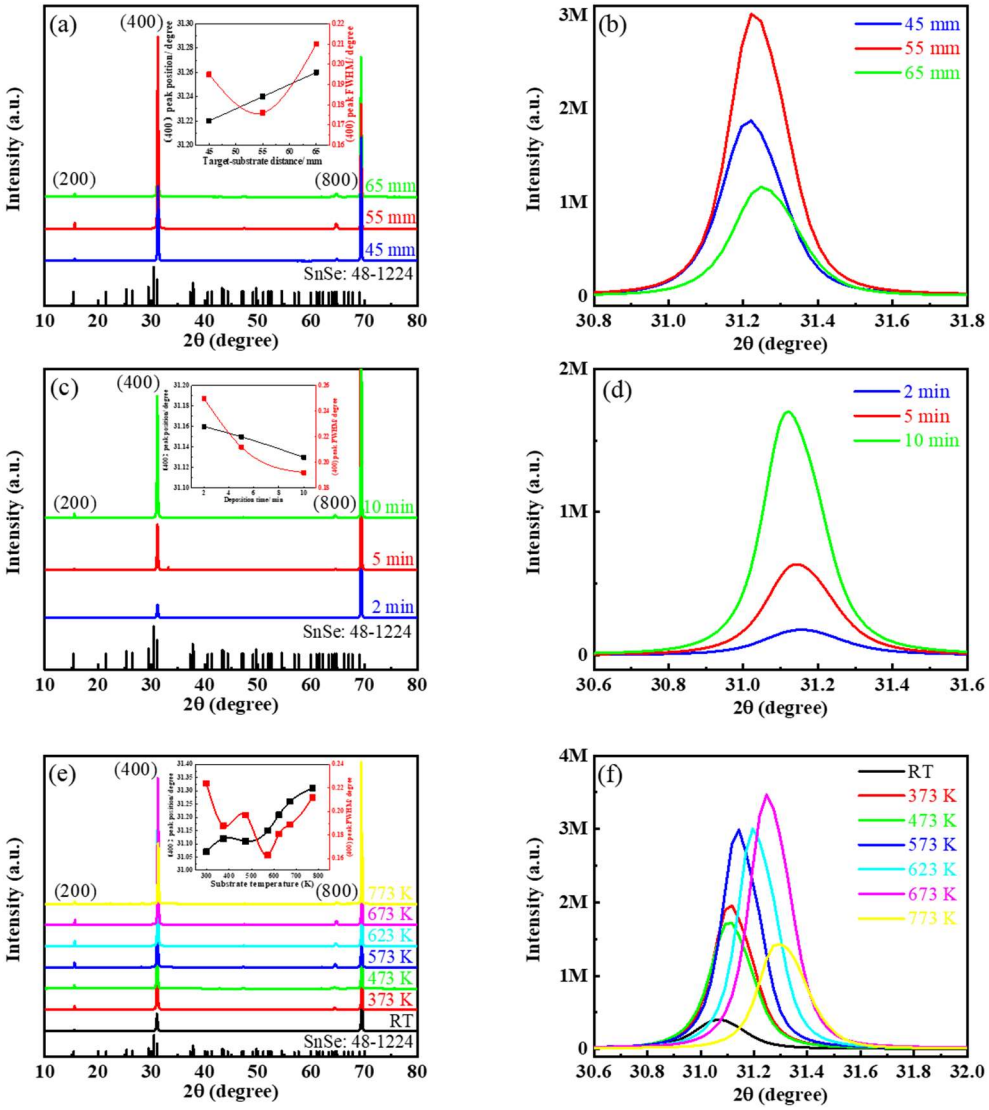

Figure S2(a) shows the XRD result of the target-to-substrate distances, the inset gives the main peak (400) peak position shifts to the higher angle and the FWHM changes with the target-to-substrate distances. **Figure S2**(b) shows the expand view of the main peak, indicating the best crystalline of the film is obtained with the 55 mm distance.

Figure S2(c) shows the XRD result of the deposition time based on the 55 mm distance, the inset demonstrates the main peak (400) peak position shifts to the lower angle and the FWHM decrease with the increasing deposition time. **Figure S2**(d) shows the expand view of the main peak. indicating the best crystalline of the film is achieved with deposition time of 10 min.

Figure S2(e) shows the XRD result as a function of deposition temperature with target-to-substrate distances of 55 mm and deposition time of 10 min. Clearly, the main peak position shifts to the higher angle with the increasing temperature. **Figure S2**(f) shows the expand view of the (400) peak, and the strongest intensity was obtained at the deposition temperature at 673 K.

Therefore, the best as-deposited SnSe thin film is obtained at the 55 mm target-to-substrate distance, deposition time of 10 min and the deposition temperature of 673 K. This as-prepared thin film is used to post-anneal to further improve film quality.

Figure S3 (a) Raman mapping of the 5 × 5 mm^2 area of the SnSe film which was annealed at 673 K. (b) 20 Raman spectra were obtained from the points which were selected in the **Figure S3**(a).